Ultrasonics xxx (2014) xxx–xxx

Contents lists available at ScienceDirect

Ultrasonics

journal homepage: www.elsevier.com/locate/ultras

Picosecond acoustics method for measuring the thermodynamical properties of solids and liquids at high pressure and high temperature

F. Decremps [a,*], M. Gauthier [a], S. Ayrinhac [a], L. Bove [a,c], L. Belliard [b], B. Perrin [b], M. Morand [a], G. Le Marchand [a], F. Bergame [a], J. Philippe [a]

[a] Institut de Minéralogie et Physique des Milieux Condensés, Université Pierre et Marie Curie, 75252 Paris, France
[b] Institut des NanoSciences de Paris, Université Pierre et Marie Curie, 75252 Paris, France
[c] Ecole Polytech. Fed. Lausanne, Inst. Condensed Matter Phys., EPSL, CH-1015 Lausanne, Switzerland

ARTICLE INFO

Article history:
Received 9 December 2013
Received in revised form 13 March 2014
Accepted 2 April 2014
Available online xxxx

Keywords:
Equation of state
Melting curve
Iron
Mercury
Silicon

ABSTRACT

Based on the original combination of picosecond acoustics and diamond anvils cell, recent improvements to accurately measure hypersonic sound velocities of liquids and solids under extreme conditions are described. To illustrate the capability of this technique, results are given on the pressure and temperature dependence of acoustic properties for three prototypical cases: polycrystal (iron), single-crystal (silicon) and liquid (mercury) samples. It is shown that such technique also enables the determination of the density as a function of pressure for liquids, of the complete set of elastic constants for single crystals, and of the melting curve for any kind of material. High pressure ultrafast acoustic spectroscopy technique clearly opens opportunities to measure thermodynamical properties under previously unattainable extreme conditions. Beyond physics, this state-of-the-art experiment would thus be useful in many other fields such as nonlinear acoustics, oceanography, petrology, in of view. A brief description of new developments and future directions of works conclude the article.

1. Introduction

Acoustic properties of solids and liquids are very sensitive to subtle changes in local or long-range order which thus makes experimental measurements of phonon velocities under high pressure one of the most useful probes in condensed matter physics. Thereby, and from a very general point of view, acoustic data under extreme conditions appear to be a key parameter to unveil how physical properties evolve at high density. The first part of this article will illustrate and present some of the most important thermodynamical arguments in favor of such studies.

The second part of the article deals with technical aspects in acoustic measurements under extreme conditions. A brief review of what could be performed up to know is given, as well as a description of the main limitations. Thereafter, the article will be focused on a review of recent technical developments, the picosecond acoustics in diamond anvils cell, illustrated by experimental results obtained by our group. The principle of diamond anvils cell, i.e. the most powerful high pressure apparatus, will be first defined, followed by a description of its integration within a picosecond acoustics set-up. A summary of the different analysis methods to extract the sound velocity from the raw experimental data is also proposed. Finally, a review of few examples of previously studying samples (Hg, Si and Fe) is given in order to illustrate the capabilities of this set-up. More in general, we will show that the here-presented technique allows detailed elastic and viscoelastic studies under extreme thermodynamic conditions on a wide variety of systems as liquids, crystalline or polycrystalline solids, metallic or not, with very broad applications standing from Earth and planetary science (e.g. chemical composition of the Earth's core) to theoretical study of liquid state (e.g. development of model to account for metallic liquids behaviors).

2. Acoustics at high pressure: general arguments

Condensed matter physics under extreme conditions is a fascinating field which handles fundamental properties of solids and liquids as structural stability, magnetic and electronic transition, or phonons dynamics. To give an idea of the relevancy of pressure as tuning thermodynamical parameter, a simple argument can be found through the basic definition of the Gibbs free energy for a closed system, defined as $dG = -SdT + VdP$ with obvious notation.

* Corresponding author at: Institut de Minéralogie et Physique des Milieux Condensés, Université Pierre et Marie Curie, 75252 Paris, France. Tel.: +33 671911494.
E-mail address: frederic.decremps@upmc.fr (F. Decremps).

http://dx.doi.org/10.1016/j.ultras.2014.04.011
0041-624X/

At constant temperature, the variation of the total energy change for a given pressure shift ΔP is:

$$\Delta G = V_0 B(1 - e^{-\Delta P/B}) \quad (1)$$

where V_0 is the molar volume at ambient pressure and B the bulk modulus.

Thus, for a pressure variation of 100 GPa and a typical value of bulk modulus for a solid (say 150 GPa), a calculation gives ΔG around 3 eV, say almost 3 order of magnitude higher than a corresponding energy shift for $\Delta T = 1000$ K at ambient pressure (*i.e.* 90 meV).

To focus on the acoustic properties, the measurement of sound velocity v versus pressure (and thus of the elastic moduli C_{ijkl}, considering the Christoffel equation) enables to probe with a high sensitivity the repulsive part of the interatomic potential, i.e. the most unknown part of the internal energy U. In the adiabatic case ($\Delta S = 0$), the Maxwell definition of an elastic constant gives:

$$C^S_{ijkl} = \left(\frac{\partial^2 U}{\partial \eta_{ij} \partial \eta_{kl}}\right)_S \quad (2)$$

where η is the strain tensor. This last equation illustrates why acoustic properties of solids and liquids are very sensitive to subtle changes in local or long-range order, and why measurements of phonons velocity under high pressure are considered as one of the most useful probe of interatomic potentials variations.

Elasticity of stressed material also provides crucial insight in the thermodynamics of condensed matter through the determination of the structural stability, the pressure dependence of the density, the melting curve, the piezoelectric properties, or the mechanical properties as few examples. However, for many years, inherent problems of carrying out elastic measurements in high pressure and high temperature cells have prevented acoustics experiments under extreme thermodynamic conditions. Consequently, little is still known about acoustic properties of liquids and solids at high density, data of major interest for physics, chemistry and planetology (Fig. 1). For what concerns the last case, the argument is straightforward: taking into account that the deepest core sampling has been extracted at a depth of only few kilometers, more than 99% of the Earth interior remains to be investigated by reproducing the thermodynamic conditions in the laboratory. For example, knowledge of the Earth interior composition involves the comparison of velocity-depth models derived from seismic data with sound velocities measured under extreme conditions (hundreds of GPa) in the laboratory.

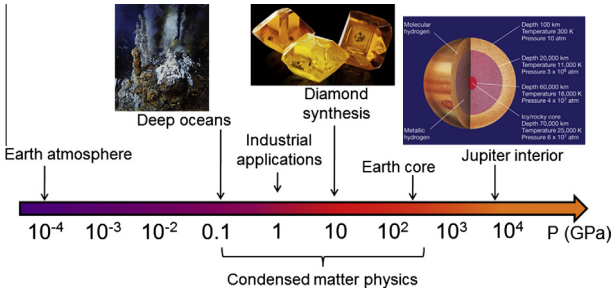

Fig. 1. Typical range of hydrostatic pressures in the field of condensed matter studies (i.e. excluding plasma state) that can be reached in laboratory with high pressure apparatus. Examples as illustration of some research issues are given. Among all, understanding the Earth interior is one of the most direct application of high pressure work in the [0–300 GPa] range (1 GPa = 10 kbar).

3. Measuring techniques

3.1. Acoustics at high pressure and temperature: a pertinent experimental tool but a challenging choice

Three types of techniques have been mainly used to measure the sound velocity of high density solids and liquids in laboratory. The first one is usually denoted as the conventional pulse-echo ultrasonic technique [1], where the typical sample thickness has to be higher that several hundred of microns to avoid successive acoustic echoes to overlap. This last constraint is the main reason why such technique can only be performed combined with a large-volume cell [2,3] (experimental volume of about 10 mm^3) limiting the highest pressure that can be reached to about 20 GPa. Secondly, GHz interferometry has been implemented [4] to measure the ultrasonic sound velocity in diamond anvils cell (DAC). Whereas this technique is a very versatile and promising method, the accurate measurement of sound velocity at high pressure still suffers from effects of quasi-hydrostatic pressure as soon as the pressure transmitting medium (PTM) solidifies (at about few GPa). The third well known method is the Brillouin scattering which can easily be adapted to be performed in a DAC [5]. However, transparent sample can exclusively be studied if sound velocities of bulk waves have to be measured. Finally, in spite of many efforts to improve the pressure range, all these constraints preclude nowadays studying the elastic and visco-elastic properties in laboratory of opaque materials under pressure above 20 GPa.

Using a novel approach which combined picosecond ultrasonics technique [6] and diamond anvils cell, we have recently shown that an original laboratory set-up circumvents all previous limitations [7–9]. Measurements of acoustic travel time are possible by this method up to 100 GPa (million of atmospheres) pressures. The main other advantages can be summarized as follows. This techniques covers a large frequency range (from 1 GHz to 300 GHz) that bridges the frequency gap between the usual laboratory techniques (from 1 MHz to 30 GHz with ultrasonics and Brillouin scattering) and the large instruments one (from 1 to 10 THz for inelastic neutron or X-ray scattering). It is a non-contact (thus without bonding effect) generation-detection technique. It opens a way of determining acoustic attenuation pressure dependence. And, last but not least, it can be applied to the study of any materials, as will be shown in the next sections. The overall feasibility of extending applications of laser ultrasonics to moderate pressures (below 30 GPa) has been recently demonstrated, in the picosecond time scale Decremps et al. [9], and in the nanosecond time scale Chigarev et al. [10,11], for the determination of sound velocity, or, using time-domain thermoreflectance in DAC, for heat transfer determination [12]. However, we here emphasize that the generation and detection of transversal waves using the picosecond technics still remains a quite challenging task. Whereas our study on single-crystalline silicon shows that, under some particular conditions, sound waves of transversal modes can be measured using picosecond acoustics in DAC, this last point has still to be considered as one of the most important limitation.

In the following, DAC and time-resolved picosecond optical principles will be first described. The capability of their combination will then be demonstrated through the high pressure generation and detection of hypersonic sound waves in a polycrystal of iron, a single-crystal of silicon, and a liquid of mercury.

3.2. Diamond anvils cell

The diamond anvils cell offers many advantages and is commonly considered as the most efficient high static pressure generator. First, it benefits of the diamond strength, secondly it offers relatively ready access to light with a large range of frequencies.

Please cite this article in press as: F. Decremps et al., Picosecond acoustics method for measuring the thermodynamical properties of solids and liquids at high pressure and high temperature, Ultrasonics (2014), http://dx.doi.org/10.1016/j.ultras.2014.04.011

The sample can be observed optically, and its reflectivity measured with infrared, visible or ultraviolet wavelengths. Raman or fluorescence spectroscopy can therefore be also performed.

As shown in Fig. 2, two beveled diamonds, previously cut with truncated flat culets, are pressed in front one to the other, a metal gasket being placed between to confine the sample in a pseudo-hydrostatic environment. Hydrostaticity can be achieved by filling the experimental volume with an inert gas. Rare gases (as neon or argon) have been here used as pressure transmitting medium. Pressure is tuned by the force applied to the diamonds through the deformation of a membrane. At ambient temperature, P is usually measured using the fluorescence emission of a μm ruby sphere [13] placed close to the sample into the gasket hole. The accuracy is typically better than 1%. At high temperature, P is determined by the shift of the $SrB_4O_7:Sm^{2+}$ fluorescence line which is known to be temperature independent [14] (accuracy similar to the ruby fluorescence shift method). To reach high temperatures the DAC is placed in a resistive furnace. The relative uncertainty on the temperature is estimated around 1%.

3.3. Experimental set-up

Picosecond acoustics is a nondestructive pump–probe experiment which belongs to the class of modern ultrafast optical methods used for about twenty years, mainly carried out to measure the mechanical and thermal properties of thin-film materials [15]. It is thus a well-adapted technique to study micrometer dimensions samples embedded in a DAC.

In our set-up, described in Fig. 3, ultrashort pulses of 100 fs are generated every 12.554 ns by a Ti:Sapphire laser (800 nm). The laser beam is split into pump and probe beams. The pump is focused on one surface of the sample, whereas the probe is focused on the opposite one. As soon as the pump laser pulse reaches the surface, it creates a sudden and small temperature rise (of about 1 K). The corresponding stress generated by thermal expansion relaxes by launching acoustic strain fields.

After propagation along the sample, both thermal and acoustic effects alter the optical reflectivity of the sample in two ways: the photo-elastic effect, and the surface displacement (as the acoustic echo reaches the surface). The first modification contributes to the change of both real and imaginary parts of the reflectance, whereas the second one only modifies the imaginary contribution. In a pure thermo-elastic model, the time and space reflectivity change $\Delta r(t)$ can be represented for a given propagation k_0 as a function of the photo-elastic coefficient $\partial n/\partial z$ (n is the optical index of the sample and z the light penetration depth) and the surface displacement $u_0(t)$ as:

$$\frac{\Delta r(t)}{r_0} = ik_0\left\{2u_0(t) + \frac{\partial n}{\partial z}\frac{4n}{1-n^2}\int_0^{+\infty}\eta(z,t)e^{2ik_0nz}\,dz\right\} \tag{3}$$

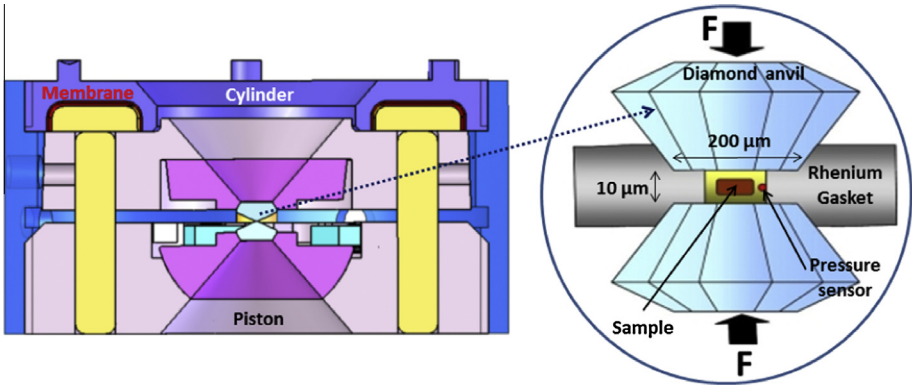

Fig. 2. Schematic diamond anvil cell principle. Diamond is chosen for its hardness and its transparency in a wide electromagnetic radiation frequency range, especially in the laser range, given an optical access to the sample. Both cylinder and piston are aligned with respect to the gasket hole. Right: Enlarged part of the high pressure environment of the DAC (by courtesy of Philippe Gillet). The sample, confined in a metallic gasket hole with the pressure sensor, is surrounded by a rare gas as pressure transmitting medium. See text for the details.

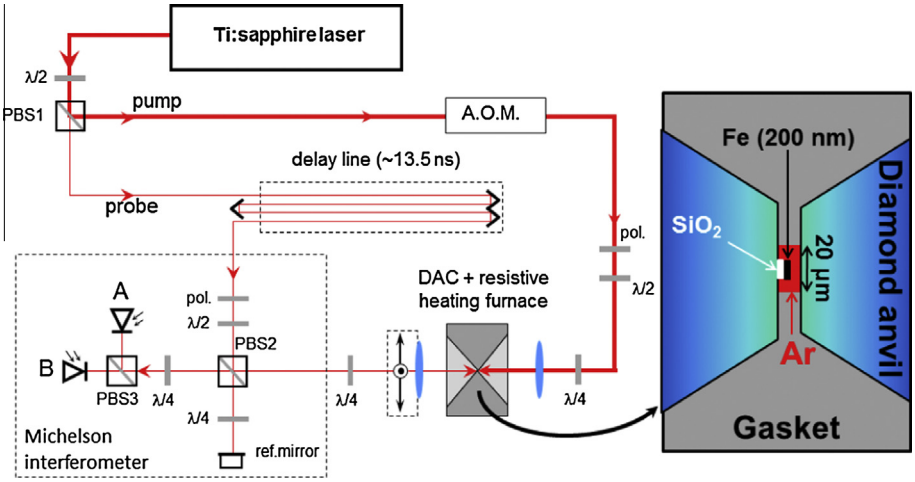

Fig. 3. Left: Schematic of the DAC/picosecond acoustics combination set-up in the transmission configuration. Here, both real and imagery part of the reflectivity are measured using a Michelson interferometer. PBS: polarizing beam-splitter, $\lambda/4$: quarter wave plate, $\lambda/2$: half-wave plate, pol.: linear polarizer, A.O.M.: acousto-optic modulator. A and B: diodes. See text for the details. Right: Enlarged part of the 200 nm thick iron sample in the DAC, surrounded by argon as pressure transmitting medium.

Please cite this article in press as: F. Decremps et al., Picosecond acoustics method for measuring the thermodynamical properties of solids and liquids at high pressure and high temperature, Ultrasonics (2014), http://dx.doi.org/10.1016/j.ultras.2014.04.011

The variation of reflectivity as a function of time is detected through the intensity modification of the probe delayed from the pump with a different optical path length. The uncertainty on the absolute position of the delay line being less than 1 μm, the determination of the pump/probe time delay is better than 20 fs. The detection is carried out by a stabilized Michelson interferometer which allows the determination of the complex reflectivity change [16].

Microscope objectives are here necessary in order to focus both pump and probe beams down to 3 μm (objectives with a typical working distance of about 20 mm and an optical aperture of 0.42, well adapted to the DAC environment, have been used). Finally, an image is obtained by scanning the reflectivity of the whole sample surface through the displacement of the probe objective in the plane perpendicular to the beam using a *X*–*Y* piezoelectric stage (giving rise to images of 100 μm × 100 μm, with an accuracy on the absolute position better than 1 μm).

The next section deals with the extraction of the sound velocity from the raw experimental data, say the time dependence of the surface sample reflectivity. As described, two distinct modifications of the experimental set-up can be used, whereas the study is focused on sample which thickness as a function of pressure is known or not.

4. Data analysis and sound velocity measurements

This section will be concerned primarily with the problem of determining the sound velocity of liquids and solids at extreme conditions by means of travel time acoustic wave measurements. Two types of measurements will here be emphasized. The so-called "temporal method", where v is determined using a similar technique as the pulse echoes one. Note that here, the knowledge of the sample thickness e is requested. This technique being one of the most frequently used methods in ultrasonics community, it will not be considered at length in the present paper. The "imagery method" will however be described in more details. Mainly inspired by the acoustic wavefronts imaging technique developed in the 1990s [17], we would here particularly stress our development of a new type of analysis, which enables the determination of both v and e at the same time and for each pressure.

4.1. Temporal method

In this first configuration, similar as the one used in a classical sonar experiment, the probe beam is focused into a spot on the opposite surface of the sample with respect to the surface illuminated by the pump, the two beams being collinear. The variation of reflectivity as a function of time is detected through the intensity modification of the probe delayed from the pump by a different optical path length. The detection is usually carried out by a stabilized Michelson interferometer which allows the determination of the reflectivity imaginary part change (at high pressure, interferometric measurements are necessary to efficiently detect acoustic pulses with a low frequency spectrum due to sound attenuation). The surface displacement of the sample is thus here determined by scanning the reflectivity at a given (and fixed) position of the probe beam as a function of time (i.e. of the delay line position). Peaks in the reflectivity are observed as soon as the acoustic waves reaches the sample surface (see Fig. 4). The first peak obviously corresponds to a travel of the bulk wave through a single way (i.e. the thickness of the sample), followed by echoes due to several reflections at the sample interfaces.

In the present study, for each pressure and temperature condition, longitudinal acoustic echoes have been systematically observed in the recorded time variation of the reflectance imaginary part.

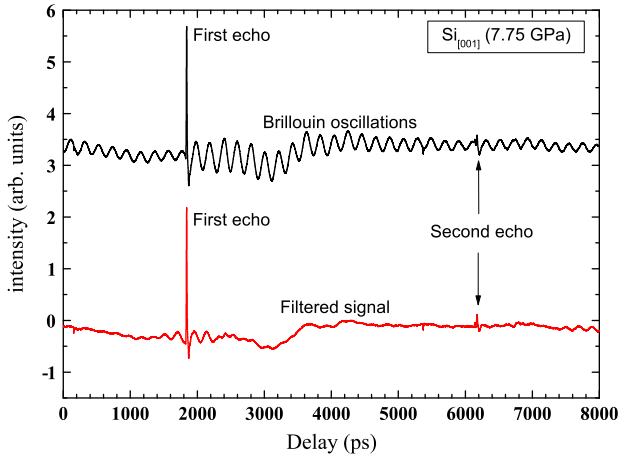

Fig. 4. Above: raw reflectivity change as a function of the optical probe-pulse time delay of a single crystal of silicon along the [1 0 0] propagation direction at 7.75 GPa. First and second echoes of the longitudinal acoustic wave can be detected. The time Δt needed for traveling from one surface of the sample to the opposite one corresponds to the time difference between the occurrence of these two echoes. Below: same signal but processed through a band block filtering at the frequency of the Brillouin interferences between the probe beam and the acoustic wave in the pressure transmitting medium.

The sound velocity v as a function of pressure was derived using this so called "temporal method" from the pressure variations of Δt using the equation:

$$e_0 = v\Delta t = v(t_0 + pT_{laser} - \tau) \quad (4)$$

where e_0 is the sample thickness (the subscripted "0" indicates that the measurement is carried out with a particular and fixed spatial position of the probe, i.e. in the axis of the pump beam). t_0 is the corresponding emergence time of the wave at the surface of the sample at a given pressure. In order to relate t_0 to the relevant travel time Δt, it is here required to determine p and τ. The integer p takes into account the successive generation of echoes due to the laser repetition rate (12.554 ns), and the value of τ corresponds to the time at which the pump–probe coincidence occurs. p value is easily assigned taken into account a rough estimated value of the travel time. For what concerns τ, it is previously measured using an aluminum thin film outside and inside the DAC (the variation of the optical path due to the presence of diamonds DAC, around 2 mm thick is negligible). For the present set-up, we determined $\tau = 0.330 \pm 0.002$ ns.

For each pressure, the longitudinal velocity v_L has thus been determined using Eq. (4). The values of e_0 at high pressure cannot be determined *i* this configuration. However, it may be deduced from its ambient pressure value and its equation of state (EOS) which can usually be easily found in the literature (through X-ray diffraction for example, assuming the isothermal and adiabatic bulk modulus to be equal). Note that this procedure, mainly used in classical ultrasonic measurements (say, with the use of a piezoelectric transducer), does not affect the accuracy of the sound velocity measurements. As a matter of fact, it is well known empirically that for a given pressure variation, when Δt is varying for about 10%, e_0 does not vary more than 1%. The variation of v_L with P is thus mainly given by the pressure dependence of the travel time Δt.

Whereas this configuration allows a simple and quick[1] way to extract the sound velocity, its major and evident disadvantages come from:

(i) the need for the sample EOS (to get the thickness, which has to be known or calculated at each thermodynamical conditions);

[1] Typically, the whole set of raw reflectivity data represented in Fig. 4 has been recorded within a couple of seconds.

Please cite this article in press as: F. Decremps et al., Picosecond acoustics method for measuring the thermodynamical properties of solids and liquids at high pressure and high temperature, Ultrasonics (2014), http://dx.doi.org/10.1016/j.ultras.2014.04.011

(ii) as the laser illuminates the sample with a spot size much higher than acoustic wave length, the acoustic propagation may be considered to be essentially that of a plane wave, and only longitudinal acoustic strain field is created.

We thus have slightly modified our set-up in order to be able to record the 2-D reflectivity of the sample surface under pressure as a function of time. This improvement, called "imagery method", enables to determine experimentally as a function of pressure and temperature both sound velocities (longitudinal v_L and transverse v_T), and the thickness values e_0.

4.2. Imagery method

Original development of acoustics using small source and point detector have revealed some striking properties of phonons in anisotropic materials, such as phonon-focusing effect [18]. In crystals, the direction of acoustic energy flow does generally not coincide with the wave vector direction **k**. Consequently, a source producing an uniform angular distribution of **k** will generate an anisotropic propagation of elastic energy. Considering a crystal with plane parallel surfaces, a point acoustic source at one surface will produce non-uniform focusing pattern at the opposite face. This produces patterns related to the complex topology of the group velocity surface (also called wave surface). Such intriguing imaging can however be calculated from elastic theory (within the continuum model) taking into account the relation between directions of **k** (or phase velocity $\mathbf{v} = \omega(\mathbf{k})/\mathbf{k}$) and directions of energy flow (or group velocity $\mathbf{v}^e = \partial\omega(\mathbf{k})/\partial\mathbf{k}$). Experimentally, the earlier images of flux energy pattern, obtained in heat-pulse experiments [19], have shown that a massive amount of data may be extracted from successively recording acoustic wavefront snapshots at different times. In recent years, the technique of picosecond laser acoustics has been shown to be well suited for such purpose [20]: femtosecond duration of the laser pulse and the possibility to focalize the beams onto the surface plane [21] of the sample give rise to an outstanding resolution in space and time. In particular, the measurements of group velocities using picosecond acoustics has been shown to allow the determination of the complete set of elastic constants of anisotropic sample at ambient pressure [22]. Following this approach, and taking into account the considerable progress made the last five years in ultrafast acoustics [23], we have here implemented the wavefront imaging method in the case of picosecond acoustics in DAC.

To simply illustrate the methodology and data analysis of such method, we describe in the following the simple case of an isotropic sample without transverse mode, the liquid mercury [24]. However, the reader will find further details in Section 5 on the case of transversal acoustic waves generation-detection in a solid sample.

Liquid mercury being elastically isotropic, the pump laser generates bulk spherical wavefronts[2] which will produce circular patterns as reaching the probed surface (see Fig. 5).

A typical 100 μm × 100 μm image associated with the integrated intensity profile is shown in insets of Figs. 5 and 6. The center of the acoustics rings is spatially determined with an uncertainty lower than ±0.5 μm in the two directions perpendicular to the beam. Due to the repetition rate of the laser, these patterns are renewed every T_{laser}.

Perfect circular rings are expected in the liquid phase, taking into account that parallelism of the diamond culets remains at high pressure [25]). The solid phase of mercury (α-Hg) is easily detected since the acoustics pattern is here no longer circular due to the anisotropy of the crystal.

For each thermodynamical condition, the acoustic wavefronts pattern is recorded as a function of pump–probe delay, with a time step of 0.1 ns. All corresponding integrated profiles can be stacked together into a graph (Fig. 7) where the vertical color scale indicates the regions of high (red) and low (blue) reflectivity.

Considering the evolution of spherical wavefronts inside the sample, the time evolution of the ring diameters $R(t)$ is simply given by:

$$R(t) = \sqrt{e^2(t) - e_0^2} \tag{6}$$

where $e(t) = v(pT_{laser} + t - \tau)$ is the distance covered by the wavefront acoustics wave inside the sample.

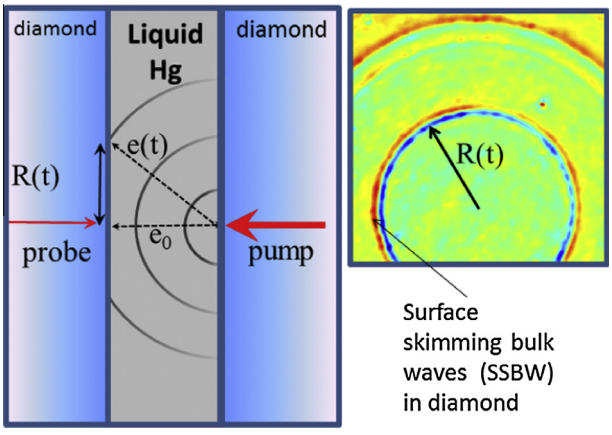

Fig. 5. Produced by the tightly focused laser beam, spherical wavefronts due to acoustics diffraction occur [24]. Consequently, the radius $R(t)$ of circles appearing on the surface depends on the sample thickness e_0 and on the straight path of the acoustic wavefront $e(t)$. (Note that diam. stands for diamond anvil).

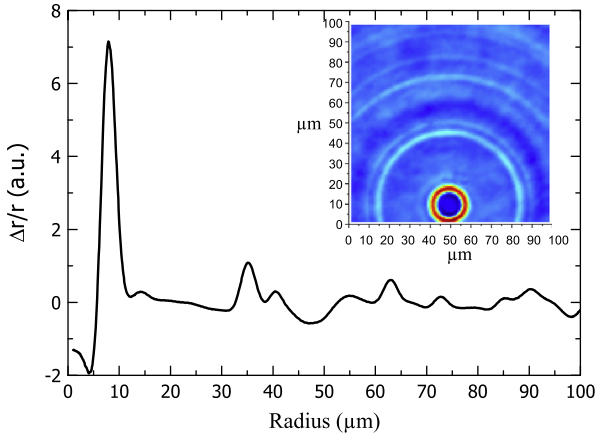

Fig. 6. Change in the reflectivity of liquid mercury at 1 GPa and 340 K as a function of the optical probe-pulse time delay [24]. Inset: corresponding experimental image of acoustic wavefront on the surface of liquid Hg with an arbitrary color scale, and associated profile integration in liquid mercury at delay t = 5.3 ns.

[2] In the source near-field, the acoustical wavefront is complex. The transition between the near-field and the far field occurs at the depth:

$$z_t \approx \frac{d^2}{4\lambda_{ac}} \tag{5}$$

where d = 3 μm is the diameter of the laser spot and λ_{ac} the mean wavelength of the acoustic wave packet. In our set-up, the mean frequency of the wave packet extracted from a Fourier transform of a temporal scan is roughly 0.6 GHz leading to $\lambda_{ac} \approx 1$ μm. The transition distance $z_t = 2$ μm is thus well lower than the sample thickness which simplifies the analysis of the detection process, done in the far field approximation.

Please cite this article in press as: F. Decremps et al., Picosecond acoustics method for measuring the thermodynamical properties of solids and liquids at high pressure and high temperature, Ultrasonics (2014), http://dx.doi.org/10.1016/j.ultras.2014.04.011

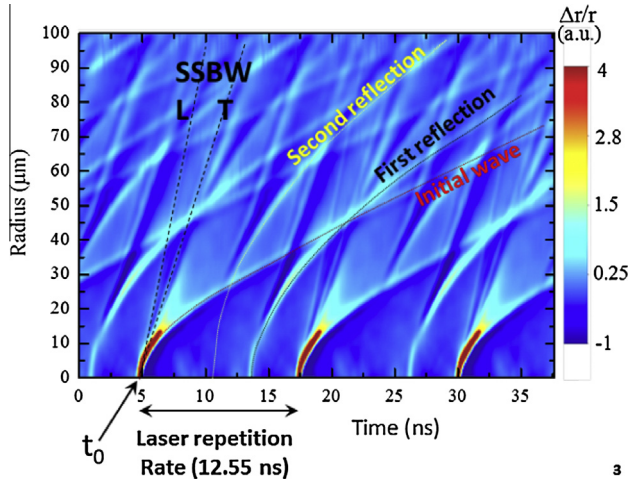

Fig. 7. Integrated profiles as a function of time at 1 GPa and 340 K. The time scale is extended by repetition of the picture each T_{laser}. The initial wavefront (red line, which is a fit of data with Eq. (6), as well as the first and second reflections (pink and green lines respectively) can be observed [24]. Note that the second reflection seems to arrive earlier than the first echo in the figure, but of course not. This comes from the folding of the pictures due to the laser repetition rate. Moreover, few ripples have a linear dependance of the radius with time, the signature of surface skimming bulk waves (SSBW) propagating in the diamond parallel to the surface (dashed lines)). These waves arise at the critical angle of the Snell–Descartes law of acoustic refraction at the diamond–mercury interface. Above this critical angle there is total reflection and any other SSBW cannot be generated. This angle is estimated at 4.3° between the propagating wave vector of the mercury bulk wave and the diamond surface. This weak angle imposes the SSBW are generated roughly at t_0. In interferometry two kinds of SSBW are visible with mean velocities of $c_T = 12 \pm 1$ km/s and $c_L = 18 \pm 1$ km s^{-1} corresponding to the transverse and longitudinal velocities in diamond, as expected. (For interpretation of the references to colour in this figure legend, the reader is referred to the web version of this article.)

Eq. (6) is fitted to the experimental points (Fig. 7) with the sound velocity v and the arrival time t_0 as free parameters. The experimental radius are deduced from the integrated profile of each pattern. Note that the determination of the exact radius of the rings has to be done taking into account the nonzero thickness of the wavefront. The bipolar profile can be understood taken into account the generation, propagation and detection process involving the acoustic pulse. The exact theory is beyond the scope of this paper however a brief explanation can be proposed. The thermoelastic generation in the liquid Hg (in contact with the diamond anvils) produces an unipolar and asymmetric strain profile [26]. During its propagation from the near field to the far field, the acoustic pulse transforms from unipolar to bipolar shape. This transformation is explained by the Gouy phase shift due to acoustic diffraction [27]. Finally, one can concluded that the shape of the echo in the signal is related to the shape of the pulse [26].

This imaging configuration is thus very powerful: both thickness and sound velocity of the sample are determined using a self consistent method. But it has the main disadvantage to be very time consuming: about 5 h per point are required, while seconds are needed by the "temporal method").

We thus only used the imagery method at few pressures (about three or four pressures per isotherms) in order to extract both v and e_0 for each point. Downstroke, we observed a weak pressure dependence of the thickness, as previously published [28]. Thus, a simple linear interpolation of these experimental points is used and provides a reliable estimation of the thickness variation as a function of pressure for the whole pressure and temperature range of the experiments.

Then the sample thickness being known, the sound velocity can be directly extracted in a short time period for many other pressure points using the "temporal method".

5. Measurement of sound wave velocity of polycrystalline iron at high pressure

Experiments at conditions of planetary's core are still extremely challenging and important topics addressed include the density, the magnetism, and of course the sound velocity at ultrahigh pressures. Among all, the elastic properties of iron, particularly reference to get a better understanding of the Earth's core, have been the subject of several papers. However, a huge discrepancy exists between shock waves non-equilibrium experiments [29] and indirect measurements of sound velocity under static compression [30].

In this study [31], the diamond anvil cell device combined with the technique of picosecond ultrasonics is demonstrated to be an adequate tool to measure the acoustic properties of iron up to 152 GPa, i.e. one order of magnitude higher than previously published ultrasonic data. A disk of iron with 10 μm of diameter has been deposited on a platelet of silica 5 μm thick (see right part of Fig. 3). Loaded in a DAC (diamonds with culet of 100 μm and bevel of 300 μm), the quality of the iron sample has been first checked through X-ray diffraction, giving rise to homogeneous diffraction rings (i.e. excellent polycristallinity) and the expected density $\rho = 7.85(1)$ g cm^{-3}). The grain size of the polycristalline iron sample was less that 1 μm –.

Using the well known acoustic velocity of bcc iron at ambient conditions [32] and the travel time value from picosecond measurement at ambient conditions, the thickness of the iron disk was measured to be 203(1) nm. Argon was used as pressure transmitting medium and the fluorescence of a ruby chip as pressure sensor. We conducted three different picosecond acoustics experiments, 152 GPa being the highest pressure reached before anvils blew out.

In this study, combining the diamond anvil cell device with the technique of picosecond ultrasonics is demonstrated to be an adequate tool to measure the acoustic properties of iron up to 152 GPa, say one order of magnitude higher than previously published ultrasonic data. The accuracy, comparable to piezoacoustics technique, allows to observe the kink in elastic properties at the bcc–hcp transition and to show with a good confidence that the Birch's law still stand up to 150 GPa and ambient temperature. At each pressure, the arrival of the first longitudinal acoustic echo (corresponding to a single-way path between the two sample surfaces, corrected by the pump/prob coincidence time, being previously measured at 33 ps) was systematically observed from the relative variation of the reflectance imaginary part (Fig. 8).

The accuracy, comparable to piezoacoustics technique, allows to observe the kink in elastic properties at the bcc–hcp transition and to show with a good confidence that the Birch's law still stand up to 150 GPa and ambient temperature (Fig. 9).

The linear extrapolation of the measured sound velocities vs densities of iron is clearly out of the PREM model, confirming that light elements should be present in the Earth's core. Beyond, this kind of experimental data applied to other geophysical relevant systems will certainly be useful in several other fields such as planetology or petrology.

6. Measurement of elastic moduli of silicon single crystals at high pressure

In the previous study on iron, where the measurement is similar to the pulse-echo ultrasonic technique (travel time determination), one of the main advantages is the use of an optical way of generation and detection (i.e. no contact and no bonding effect). However, in the acoustic far field diffraction limit (the laser illuminates the sample with a spot size much higher than the film thickness), only longitudinal acoustic strain field is created and no shear wave can be detected. In order to circumvent the "shearless" problem, we

Please cite this article in press as: F. Decremps et al., Picosecond acoustics method for measuring the thermodynamical properties of solids and liquids at high pressure and high temperature, Ultrasonics (2014), http://dx.doi.org/10.1016/j.ultras.2014.04.011

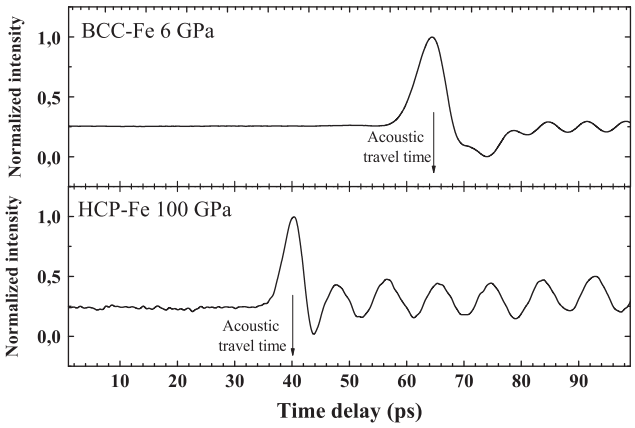

Fig. 8. Change in the normalized reflectivity imaginary part of iron at 6 GPa and 100 GPa as a function of the optical probe-pulse time delay. Due to acoustic attenuation and dispersion effects, the width of the acoustic pulse is here around 10 ps. The acoustic signal is followed by a damped oscillatory component. This contribution arises from the acousto-optic modulation of the probe beam from the propagating acoustic waves (e.g. stimulated Brillouin scattering signals). The first ps following the arrival of the iron acoustic pulse corresponds to the Brillouin oscillations due to a wave propagating in silica, followed by the same type of signal but in diamond (propagation into the anvil, within a depth of tens of microns).

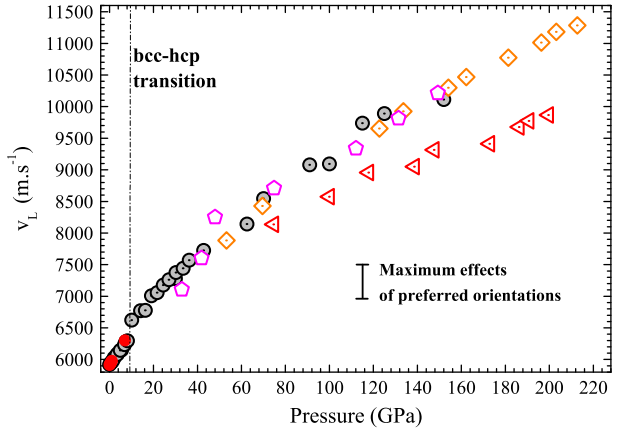

Fig. 9. Longitudinal wave velocities v_L of iron as a function of pressure for the present work (black gray filled circles) [31] and plotted along with ultrasonic from Ref. [32] (red filled circles), radial XRD measurements from Ref. [30] (orange dot center diamonds), NRIXS data from Ref. [33] (magenta hexagon) and shock wave Hugoniot measurements from Ref. [29] (red dot center left triangles). For information, the possible effects of preferred orientations at 150 GP, as estimated from [34,35], are also illustrated. (For interpretation of the references to colour in this figure legend, the reader is referred to the web version of this article.)

have generated lateral compressive stresses (producing internal diffraction) through a minimization of the source area with respect to the characteristic acoustic wavelength. The wavefront "imagery method" is then used to extract the complete set of elastic constant as a function of pressure. The prototypical case of a single crystal silicon has been studied and is shown in the following, demonstrating the high accuracy of such method.

6.1. Sample and high pressure environment

Extracted from a large single-crystal of silicon, a thin platelet oriented along [100] with surface of about $70 * 70\ \mu m^2$ was mechanically polished. A thin film (50 nm) of Al was sputtered on both sides to serve as transducers. This sample was loaded into the experimental volume of the DAC. Neon was used as pressure transmitting medium. Using the well known longitudinal velocity of Si along the [100] direction at ambient conditions [1], the thickness of the crystal platelet was measured to be 42.2(1) μm from picosecond measurement in the classical configuration (i. e. scanning the delay at fixed pump–probe relative position). Pressure was classically measured using the fluorescence emission of a 5 μm ruby sphere placed close to the sample in the gasket hole. The accuracy was better than 0.1 GPa at the maximum pressure reached.

6.2. Propagation of the acoustic energy in a cubic structure at ambient conditions. Theory and experience

Taken into account the cut of our silicon single crystal, its well known density ($\rho = 2.331\ g\ cm^{-3}$) and elastic constants values at ambient conditions, we first solved the Christoffel equation for a set of wave vectors **k** lying within 45degr (cubic symmetry) around the [100] crystallographic direction. The slowness curves are then generated for the three acoustical polarizations and, in a second step, used to calculate from ray theory [36] the wave front curves within a surface cut in the plane (100). In Fig. 10, a typical 3-D phonon imaging pattern for the three acoustic polarizations is given.

The experimental and calculated intercepts between 3-D wave front and (100) plane of silicon is shown in Fig. 11 at ambient conditions and at 7.75 GPa. The simulated process of the wave surfaces, where the elastic constants are the fitting parameters, well reproduces the experimental pattern and gives rise to an elastic tensor in very good agreement with previously published data [1,37]. We here emphasize that, for a given thermodynamical condition (ambient or high pressures), successive patterns at different pump–probe delays can be used to renew the fitting process in order to determine the complete set of elastic constants with an exceptional accuracy.

Note that the fast transversal mode was not experimentally detectable and thus not been taken into account in the elastic constants fitting process. The absence of this mode (polarized into the (100) plane) can be easily understood using Eq. (3), where the imaginary part is mainly dominated by the surface displacement perpendicular to the surface. Consequently, using our interferometric configuration, any surface displacement could be detected except when it is perpendicular to the surface. In our case (cubic structure), a calculation of a [100] projection of polarization vectors actually demonstrates the absence of the fast transversal mode for which the corresponding displacement is almost zero.

6.3. Pressure dependence of the elastic constants and equation of state of silicon

In this study, the "imagery method" has been exclusively used for each pressure point. In order to take into account the elastic anisotropy of the single crystal, the complete set of elastic

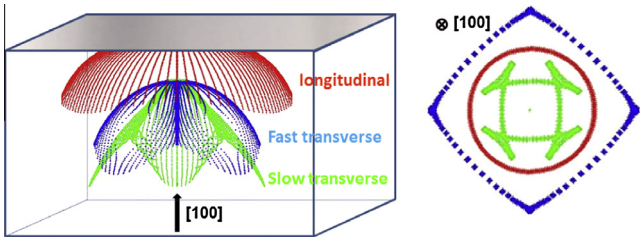

Fig. 10. Calculated group velocity surfaces near the [100] symmetry axis of ZB-cubic silicon for a time delay of 3.5 ns. Red, blue and green dashed lines correspond respectively to the longitudinal, fast and slow transversal group velocities. Right: cut surface along the (100) plane of the cubic silicon structure). (For interpretation of the references to colour in this figure legend, the reader is referred to the web version of this article.)

Please cite this article in press as: F. Decremps et al., Picosecond acoustics method for measuring the thermodynamical properties of solids and liquids at high pressure and high temperature, Ultrasonics (2014), http://dx.doi.org/10.1016/j.ultras.2014.04.011

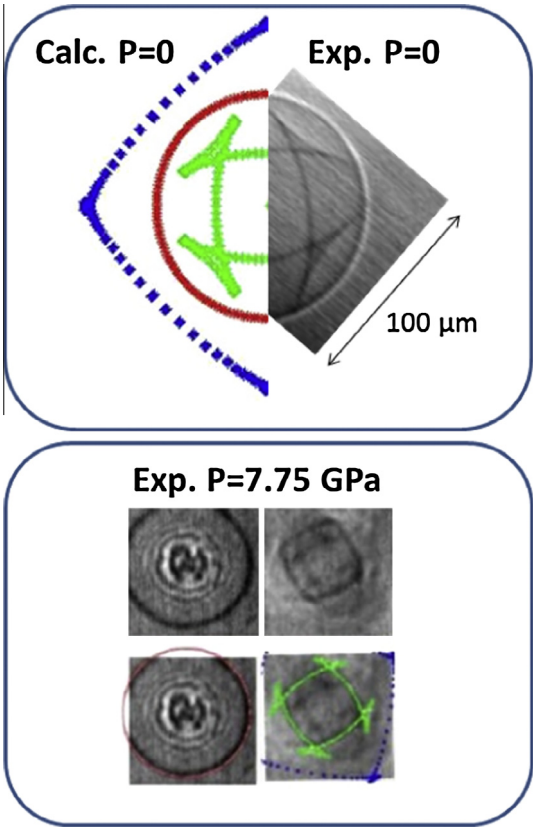

Fig. 11. Top panel: Experimental phonon imaging pattern in the (100) plane of silicon at ambient conditions (pump–probe delay time of 0.4 ns). Red, blue and green dashed lines correspond respectively to the longitudinal, fast and slow transversal group velocities using C_{11} = 165.7 GPa, C_{12} = 63.9 GPa and C_{44} = 79.5 GPa. Lower panel: experimental phonon imaging patterns in the (100) plane of silicon at 7.75 GPa at two different pump–probe delays. Bottom: same as top with superimposed calculation curves for longitudinal, fast and slow transversal group velocities (red, blue and green dashed lines respectively) using C_{11} = 196.9 GPa, C_{12} = 104 GPa and C_{44} = 80 GPa. (For interpretation of the references to colour in this figure legend, the reader is referred to the web version of this article.)

constants as well as the density of silicon have been here determined using the analysis principle described in Section 3.2 and the following procedure. Assuming that length and density are known at a given pressure P (ambient pressure, for example), all velocities and elastic moduli can be directly deduced from the picosecond measurements. Using P-values of density and thickness, and $P + \Delta P$ wavefront snapshots for different pump–probe delay, the length and the density of the sample at $P + \Delta P$ can be computed. These values are then used to deduce a first approximation of the elastic moduli at the new pressure $P + \Delta P$. The values of the latter are finally used as starting points in an iterative process, until convergence is reached. This process is quite robust since the variation of the sound velocity is mainly due to that of the elastic moduli (i.e. its dependence on length and density is only of second order).

Fig. 12 shows elastic constants of cubic diamond (ZB) silicon as a function of pressure up to the ZB $\rightarrow$ β-Sn transition (10 GPa). An excellent agreement is observed with computations results using DFT-LDA total-energy method [38]. The comparison is also very good with tight-binding simulations [39], except for C_{44} whose calculated ambient pressure value is far from the well established value of 80 GPa [40]. Whereas this discrepancy may be due to an inadequate model parametrization, a good agreement between theoretical and experimental pressure derivative of C_{44} is nevertheless observed. Present data and 1960s ultrasonics results [1,37] are also in excellent agreement (in the pressure domain where the comparison can be done, say less than 0.2 GPa). In this pressure range, the infinitesimal strain theory does not hold anymore and, within the accuracy of the measurements, second-order moduli C_{IJ} are observed to vary linearly with pressure. However, a comparison between our data at higher pressure (typically more than 3 GPa) and a linear extrapolation of the McSkimmin and Andreacht [1,37] results is worse. Beyond the classical quasiharmonic approximation, the pressure dependence of the third-order moduli C_{IJK} of silicon is here needed to interpret such disagreement. A second-order polynomial regression of present data yields to (data in GPa):

$$C_{11}(P) = 165.7 + 4.73P - 0.09P^2;$$
$$C_{12}(P) = 63.60 + 5.78P - 0.12P^2;$$

C_{44} is however unaffected by a variation of pressure, lying around 80 GPa within the experimental uncertainty.

For cubic crystals, the bulk modulus B is a simple function of the elastic constants: $B = (C_{11} + 2C_{12})/3$.

Using the experimental values of C_{IJ}(p), highly accurate and free-hypothesis equation of state $B(p)$ has been determined (see Fig. 4).

A second-order polynomial curve well reproduces the experimental pressure dependence of the bulk modulus with: $B(P) = 97.60 + 5.74P - 0.16P^2$, in excellent agreement with a fourth-order regression of the elastic energy with respect to the strain giving: $B' = dB/dP = 5.08–0.24P$.

7. Measurement of thermodynamical properties of liquid mercury under extreme conditions

Up to now, ultrasonic experiments at pressure higher than 1 GPa could not be performed on metallic liquids. We here measured the sound velocity in liquid mercury up to 512 K and 7 GPa, an excellent example of what can be achieved with the combination of picosecond acoustics and diamond anvils cell.

7.1. Sample environment

Because mercury at high pressure and high temperature is chemically very aggressive, these experiments have been carried out using a specific experimental technique. The diamond anvil cell, made of high-temperature steel, was heated by a resistive external heater. The temperature was controlled by a thermocouple glued onto the side of one anvil. Mercury was confined in a rhenium gasket, known to be chemically inert at high temperature with mercury [41]. Moreover, no reaction is expected between carbon (i.e. diamonds) and mercury [42].

Ultra-pure mercury (99.99%) was loaded into the experimental volume. A small droplet of liquid mercury is loaded in a 200 µm diameter gasket hole whose thickness is between 20 and 70 µm. The large diameter hole is chosen to avoid acoustic reflections from the edges of the gasket. The pressure was determined with an accuracy of 0.1 GPa by the shift of the SrB_4O_7:5%Sm^{2+} fluorescence line which is known to be temperature independent [14]. A ruby ball served as an additional *in situ* temperature gauge. The relative uncertainty on the temperature was estimated around 1%.

7.2. Sound velocity

Note that here, liquid mercury is fully embedded into the gasket hole. As a consequence, the "temporal method" will enable to extract the travel time Δt corresponding to a single way of the acoustic wave into mercury (fully embedded into the gasket hole between the two surfaces of the diamond culets). We thus mainly used the "imagery method", since both thickness e_0 and sound velocity v can be here determined simultaneously. We however emphasize that, while this imaging configuration is very powerful,

Please cite this article in press as: F. Decremps et al., Picosecond acoustics method for measuring the thermodynamical properties of solids and liquids at high pressure and high temperature, Ultrasonics (2014), http://dx.doi.org/10.1016/j.ultras.2014.04.011

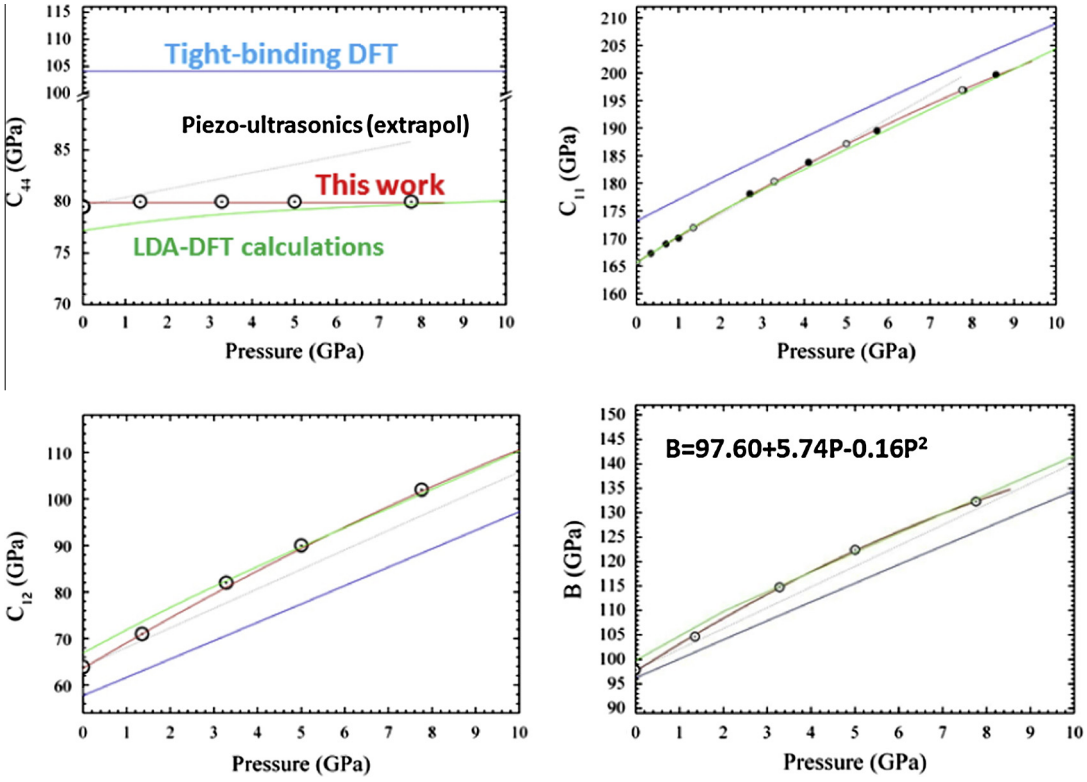

Fig. 12. Pressure dependence of cubic silicon elastic constants C_{11}), C_{44} and C_{12} at 300 K. The data for C_{11} corresponds to experiment of phonon imaging (open circles) completed by an experiment in a classical (say "temporal method") high pressure picosecond set-up. Present results (with uncertainty given by the symbol size) are compared with previous data (blue solid line: Tight-binding DFT calculations [39], green solid line: LDA-DFT calculations [38], and dot black line: extrapolation of low-pressure ultrasonics data [1,37]). The red solid line corresponds to a second-order polynomial fitting of the phonon imaging data. (For interpretation of the references to colour in this figure legend, the reader is referred to the web version of this article.)

it has the main disadvantage to be time consuming nothing compare to the couple of seconds needed by the "temporal method". We thus only used the imagery method at about four or five pressure points per isotherms in order to extract both v and e_0 for each point.

Upon the pressure downstroke we measured an almost constant value of the thickness whatever the pressure is. This observation, in agreement with previously studied [43], could be explained taken into account the complex plasticity process inside the gasket [28] under relaxing stresses. A simple linear interpolation of experimental e_0(downstroke P) values is used and provides a reliable estimation of the thickness variation as a function of pressure for the whole pressure and temperature range of the experiments. The sample thickness being known, the sound velocity can be directly extracted by a scan with temporal method.

At ambient condition, we measured a sound velocity of 1450 ± 15 m s^{-1} in good agreement with all previous studies [44–46]. Fig. 13 summarizes our complete results in pressure up to 7 GPa and temperature up to 513 K. The velocities obtained at ambient temperature and high pressures agree with the data from Davis and Gordon [46].

7.3. Equation of state

The density variations as a function of pressure and temperature can be extracted from the sound velocity measurements via classical thermodynamic relations [46–49]. The adiabatic sound velocity[3] v is related to the adiabatic compressibility by $\beta_S = 1/\rho v^2$ and to the thermal compressibility $\beta_T = 1/\rho(\partial\rho/\partial P)_T$ by

$$\beta_T = \beta_S + \frac{T\alpha_P^2}{\rho C_P} \tag{7}$$

where C_P is the isobaric heat capacity and α_P is the thermal expansion coefficient at constant pressure defined by

$$\alpha_P \equiv -\frac{1}{\rho}\left(\frac{\partial\rho}{\partial T}\right)_P. \tag{8}$$

Relation (7) can be rewritten as

$$\left(\frac{\partial\rho}{\partial P}\right)_T = \frac{1}{v^2} + \frac{T\alpha_P^2}{C_P}. \tag{9}$$

The integration of Eq. (9) between arbitrary pressures P_1 and P_2 leads to the equation

$$\rho(P_2,T) - \rho(P_1,T) = \int_{P_1}^{P_2} \frac{dP}{v^2(P,T)} + T\int_{P_1}^{P_2} \frac{\alpha_P^2(P,T)}{C_P(P,T)}\,dP \tag{10}$$

where the variation of C_P with pressure can be evaluated via

$$\left(\frac{\partial C_P}{\partial P}\right)_T = -\frac{T}{\rho}\left\{\left(\frac{\partial\alpha_P}{\partial T}\right)_P + \alpha_P^2\right\}. \tag{11}$$

The three Eqs. (8), (10) and (11) are used into the modified recursive procedure [47] described in the following in order to obtain the density as a function of pressure and temperature, shown in Fig. 14.

It is well known that equations of state (EOS) derived for the solid can also be applied to the liquid in the case of metals due to their high compressibility [53]. However, discussion still stand on the validity of physical hypothesis underlying each proposed EoS. In this work, the availability of experimentally determined

[3] The sound waves propagate adiabatically up to a frequency f given by $f = v^2\rho C_V/2\pi\kappa$ where κ is the thermal conductivity and C_V the isochoric specific heat [50]. In the liquid mercury $f \approx 100$ GHz well above the 10 GHz reached in our experiments.

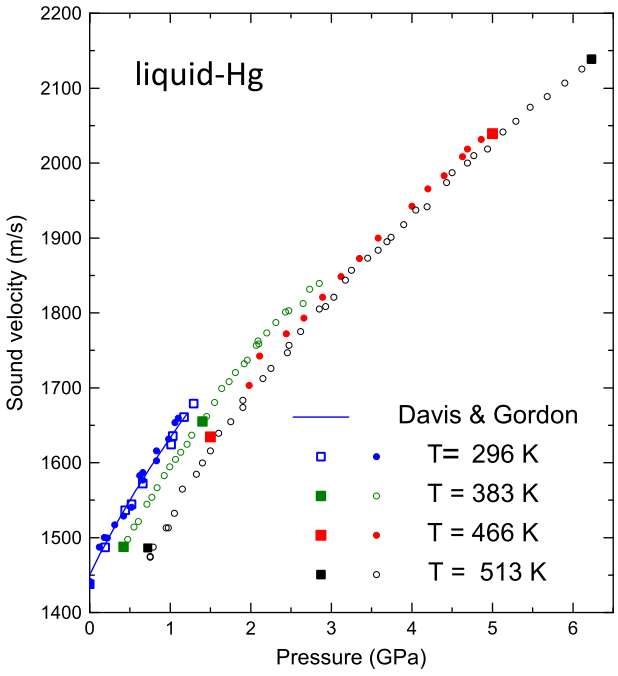

Fig. 13. Adiabatic sound velocity in liquid mercury as a function of pressure for different isotherms up to the liquid–solid transition. Squares: imagery method. Circles: temporal method. The line is from Davis and Gordon [46].

bulk modulus of liquid mercury in a wide range of pressure and temperature enables to test the validity of different stages in the development of the EOS field, for the purposes of smoothing and interpolation of pressure–volume data, and extraction of accurate values of the isothermal bulk modulus and its pressure derivative. Among them, we below described the most commonly proposed in the literature.

Use of Taylor series expansion is one of the easiest approach to develop a P–V equation in order to express pressure as a function of $\Delta V/V$. In that case, a development up to the quadratic term can be used (Davis–Gordon equation of state [54]). A similar approach is suggested in Ref. [55] where the pressure is expanded in powers ln (V) about $V = V_0$.

An alternative approach consists in formulating some hypothesis on the pressure dependence of the bulk modulus. The most simple approximation is the Murnaghan equation [56] where the bulk modulus B is considered to vary linearly with pressure ($B = B_0 + B'_0 P$), while the widely used Birch–Murnaghan EOS [57] consists in a series expansion of the free energy in terms of V.

Following the work of Rydberg [58], Vinet et al. [59] proposed an equation based on a potential with a soft repulsive contribution. In a same way, but with the assumption that at high pressure all materials are expected to convert to a Thomas–Fermi state, Holzapfel [60] proposed a modified version of the Rydberg EOS.

In order to test the validity of each of the previous EoS, we use them to calculate the pressure dependence of the volume at 513 K, using the same parameters ($B_0 = 18.5$ GPa, $B'_0 = 10.7$ and $\rho_0 = 13019.8$ kg/m^3). Finally, as a stringent test, we compare all EoS to the results of our (P,V,T) data obtained from the iterative numerical procedure described above (see Fig. 15).

As a matter of fact, the Murnaghan EOS does not reproduce our results as a strong deviation is observed in the present pressure range. Similarly, discrepancies with the Vinet and Holzapfel EOS are observed. This suggests that an hard repulsive contribution has to be taken into account to describe the behavior of liquid mercury.

Finally, one can observe that both the Birch–Murnaghan equation and the (P,V,T) Taylor series expansion proposed by Davis and Gordon can be considered as a good analytical EOS for metallic liquid, even at high density.

7.4. Melting curve

The elastic properties of all the known crystals are anisotropic. The measurement of the surface reflectance of a metal is thus expected to abruptly vary along the solid–liquid phase transition, through the change of the dielectric function, but also through the modification of the acoustic propagation modes. In the particular case of the wavefront acoustic imagery method, the difference of reflectivity pattern between the solid and the liquid phase will thus be obvious, shifting from a circle in the liquid isotropic case to a more complex shape in the solid phase (see up panel of Fig. 16).

Using this method, but also the clear modification of the temporal signal at the liquid–solid transition, we have measured the melting curve of mercury up at high pressure and high temperature. Here again, a comparison with previously published data shows a good agreement, which proves that the present technique is also well adapted to the determination of melting curve, and more generally of the phase diagram, for non-transparent materials.

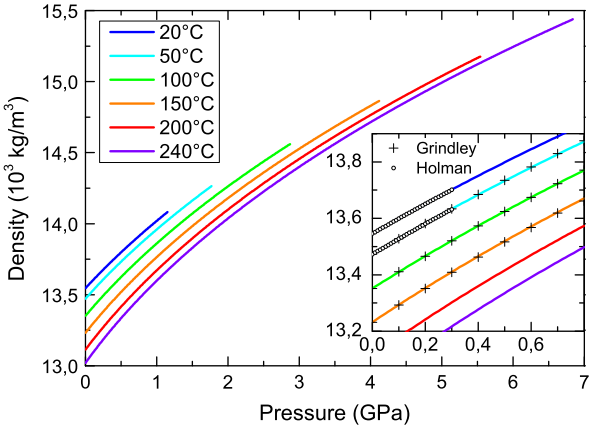

Fig. 14. Density $\rho(P,T)$ of liquid Hg versus pressure at different temperatures. The calculation procedure from sound velocity measurements is explained in the text. Inset: Comparison between our work and the data from Holman and Ten Seldam [51] and Grindley and Lind [52].

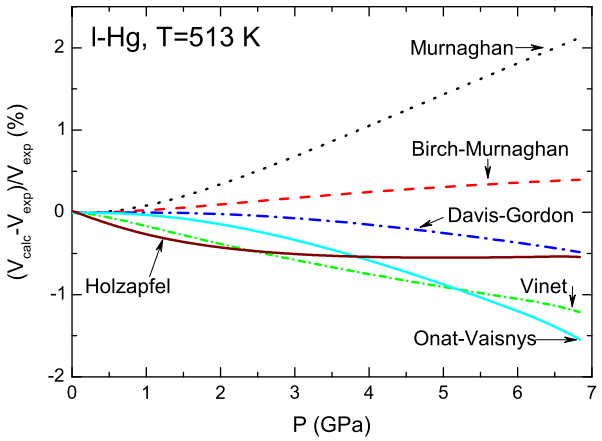

Fig. 15. Relative deviation between the experimental volume data and calculated volume obtained by the predictions of many equations of state. Physical hypothesis concerning the EOS are discussed in the text.

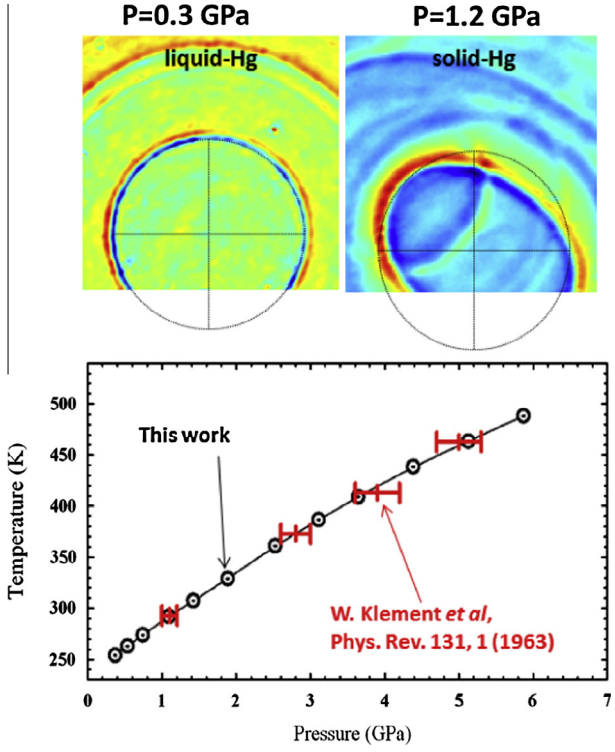

Fig. 16. Difference between the solid and the liquid phase wave front imaging of mercury at 567 K. The solid phase, elastically anisotropic, can be easily distinguished from the perfect circles arising in the liquid phase. Below: Melting curve of mercury (red crosses: present work. Black circles-line: Ref. [61]). (For interpretation of the references to color in this figure legend, the reader is referred to the web version of this article.)

8. Conclusion

Picosecond acoustic at ambient conditions is well known to be an optical pump–probe technique which enables the measurement of thermal properties of thin-film materials [6]. Here, we demonstrate that its adaptation for measurements in diamond anvil cell opens a wide landscape of new applications which would address fundamental questions centered on the thermodynamics properties of condensed matter, solids as liquids. Contrary to other groups which currently scope with these problems mostly using large facilities, we here propose entirely new and novel technique to characterize the elasticity and visco-elasticity of solid and liquid metals under such severe conditions. Briefly, through different prototypical cases of solids and liquids, we have shown that such new high pressure techniques allows the determination of:

(i) the sound velocity as a function of the density over a pressure and temperature range one order of magnitude higher than what was previously attainable;
(ii) the pressure dependence of the complete set of the elastic constants tensor;
(iii) the equation of state with a better accuracy of what is usually reached with other technics (as X-ray diffraction);
(iv) the pressure at which a solid–solid phase transition occurs in crystals;
(v) the melting curve of a metallic sample.

Application of these tools will enable in the near future to convert this technological break-through in world scientific premieres in different scientific fields, as physics but also geophysics. This obviously open new opportunities to perform spectroscopy in time domain at extreme conditions. Moreover, through the reflectance measurements (where the temperature variation of the dielectric function play a crucial role), thermal conductivity determination at high pressure is now worth considering. In particular, we may emphasize that, combining with laser heating, this technique would also open a way of determining the sound velocity under the thermodynamical conditions of the Earth's core (around 3 millions of atmospheres and 6000 K), but also the nature and way of heat and mass transfer within the interiors of the Earth and terrestrial planets.

Acknowledgments

We acknowledge P. Munsch (IMPMC) for his help during the DAC loading and F. Gelebart (IMPMC) for the objective mount conception. We also warmly thank Stefano Lun Kwong for all the manufacturing parts needed to set-up the acoustics picosecond experiment.

References

[1] H. McSkimin, P. Andreacht, Elastic moduli of silicon vs hydrostatic pressure at 25 degrees C and −195.8 degrees C, J. Appl. Phys. 35 (1964) 2161–2168.
[2] B. Li, G.D. Gwanmesia, R.C. Liebermann, Sound velocities of olivine and beta polymorphs of Mg_2SiO_4 at earth's transition zone pressures, Geophys. Res. Lett. 23 (1996) 2259–2262.
[3] M. Gauthier, D. Lheureux, F. Decremps, M. Fischer, J.P. Iti, G. Syfosse, A. Polian, High-pressure ultrasonic setup using the paris-edinburgh press: elastic properties of single crystalline germanium up to 6 GPa, Rev. Sci. Instrum. 74 (2003).
[4] A.K.S.D. Jacobsen, H.J. Reichmann, H. Spetzler, Advances in high-pressure technology for geophysical applications, in: J. Chen, Y. Wang, T.S. Duffy, G. Shen, L. Dobrzhinetskaya (Eds.), Cambridge University Press, 2005.
[5] F. Decremps, F. Datchi, A. Polian, Hypersonic velocity measurement using Brillouin scattering technique. Application to water under high pressure and temperature, Ultrasonics 44 (2006) E1495–E1498.
[6] H. Maris, Picosecond ultrasonics, Sci. Am. 278 (1998) 86–89.
[7] F. Decremps, L. Belliard, M. Gauthier, B. Perrin, Equation of state, stability, anisotropy and nonlinear elasticity of diamond-cubic (ZB) silicon by phonon imaging at high pressure, Phys. Rev. B 82 (2010).
[8] F. Decremps, L. Belliard, B. Couzinet, S. Vincent, P. Munsch, G. Le Marchand, B. Perrin, Liquid mercury sound velocity measurements under high pressure and high temperature by picosecond acoustics in a diamond anvils cell, Rev. Sci. Instrum. 80 (2009).
[9] F. Decremps, L. Belliard, B. Perrin, M. Gauthier, Sound velocity and absorption measurements under high pressure using picosecond ultrasonics in a diamond anvil cell: application to the stability study of AlPdMn, Phys. Rev. Lett. 100 (2008).
[10] N. Chigarev, P. Zinin, L.-C. Ming, G. Amulele, A. Bulou, V. Gusev, Laser generation and detection of longitudinal and shear acoustic waves in a diamond anvil cell, Appl. Phys. Lett. 93 (2008) 181905.
[11] N. Chigarev, P. Zinin, D. Mounier, A. Bulou, L. Ming, T. Acosta, V. Gusev, Analysis of ultrasonic echoes induced by pulsed laser action on iron film in a diamond anvil cell, High Press. Res. 30 (2010) 78.
[12] W.-P. Hsieh, A.S. Lyons, E. Pop, P. Keblinski, D.G. Cahill, Pressure tuning of the thermal conductance of weak interfaces, Phys. Rev. B 84 (2011) 184107.
[13] H.K. Mao, J. Xu, P.M. Bell, Calibration of the ruby pressure gauge to 800 kbar under quasi-hydrostatic conditions, J. Geophys. Res.: Solid Earth 91 (1986) 4673–4676.
[14] F. Datchi, R. LeToullec, P. Loubeyre, Improved calibration of the SrB_4O_7:Sm^{2+} optical pressure gauge: advantages at very high pressures and high temperatures, J. Appl. Phys. 81 (1997) 3333–3339.
[15] C. Thomsen, H.T. Grahn, H.J. Maris, J. Tauc, Surface generation and detection of phonons by picosecond light pulses, Phys. Rev. B 34 (1986) 4129–4138.
[16] B. Perrin, C. Rossignol, B. Bonello, J. Jeannet, Interferometric detection in picosecond ultrasonics, Physica B 263 (1999) 571–573.
[17] J. Wolfe, Acoustic wave-fronts in crystalline solids, Phys. Today 48 (1995) 34–40.
[18] B. Taylor, H.J. Maris, C. Elbaum, Phonon focusing in solids, Phys. Rev. Lett. 23 (1969) 416–419.
[19] H.J. Maris, Phonon Scattering in Condensed Matter, Plenum, New York, 1980.
[20] S. Zhang, E. Peronne, L. Belliard, S. Vincent, B. Perrin, Three-dimensional acoustic wavefront imaging in anisotropic systems by picosecond acoustics, J. Appl. Phys. 109 (2011).
[21] T. Bienville, L. Belliard, P. Siry, B. Perrin, Photothermal experiments in the time and frequency domains using an optical near field microscope, Superlattices Microstruct. 35 (2004) 363–374. Eurotherm 75 'Microscale Heat Transfer 2'.
[22] B. Audoin, C. Bescond, M. Deschamps, Measurement of stiffness coefficients of anisotropic materials from pointlike generation and detection of acoustic waves, J. Appl. Phys. 80 (1996) 3760–3771.

Please cite this article in press as: F. Decremps et al., Picosecond acoustics method for measuring the thermodynamical properties of solids and liquids at high pressure and high temperature, Ultrasonics (2014), http://dx.doi.org/10.1016/j.ultras.2014.04.011

[23] C. Rossignol, J.M. Rampnoux, M. Perton, B. Audoin, S. Dilhaire, Generation and detection of shear acoustic waves in metal submicrometric films with ultrashort laser pulses, Phys. Rev. Lett. 94 (2005) 166106.
[24] S. Ayrinhac et al., Equation of state of liquid mercury to 520 K and 7 GPa from acoustic velocity measurements, J. Chem. Phys. (2014) (in press).
[25] R.J. Hemley, H.-K. Mao, G. Shen, J. Badro, P. Gillet, M. Hanfland, D. Häusermann, X-ray imaging of stress and strain of diamond, iron, and tungsten at megabar pressures, Science 276 (1997) 1242–1245.
[26] O.B. Wright, B. Perrin, O. Matsuda, V.E. Gusev, Optical excitation and detection of picosecond acoustic pulses in liquid mercury, Phys. Rev. B 78 (2008) 024303.
[27] N. Holme, B. Daly, M. Myaing, T. Norris, Gouy phase shift of single-cycle picosecond acoustic pulses, Appl. Phys. Lett. 83 (2003) 392–394.
[28] D. Dunstan, Theory of the gasket in diamond anvil high-pressure cells, Rev. Sci. Instrum. 60 (1989) 3789–3795.
[29] J. Brown, R. Mcqueen, Phase-ransitions, Gruneisen-parameter, and elasticity for shocked iron between 77-GPa and 400-GPa, J. Geophys. Res. – Solid Earth Planets 91 (1986) 7485–7494.
[30] H. Mao, J. Shu, G. Shen, R. Hemley, B. Li, A. Singh, Elasticity and rheology of iron above 220 GPa and the nature of the Earth's inner core, Nature 396 (1998) 741–743.
[31] F. Decremps et al., Sound velocity of iron up to 152 GPa by picosecond acoustics in diamond anvil cell, Geophys. Res. Lett. 41 (2014) 1459–1464.
[32] M. Guinan, D. Beshers, Pressure derivative of elastic constants of alpha-iron to 10 Kbs, J. Phys. Chem. Solids 29 (1968) 541–&.
[33] H. Mao, J. Xu, V. Struzhkin, J. Shu, R. Hemley, W. Sturhahn, M. Hu, E. Alp, L. Vocadlo, D. Alfe, G. Price, M. Gillan, M. Schwoerer-Bohning, D. Hausermann, P. Eng, G. Shen, H. Giefers, R. Lubbers, G. Wortmann, Phonon density of states of iron up to 153 gigapascals, Science 292 (2001) 914–916.
[34] L. Stixrude, R. Cohen, High-pressure elasticity of iron and anisotropy of earths inner-core, Science 267 (1995) 1972–1975.
[35] H. Wenk, S. Matthies, R. Hemley, H. Mao, J. Shu, The plastic deformation of iron at pressures of the Earth's inner core, Nature 405 (2000) 1044–1047.
[36] B.A. Auld, Acoustic fields and waves in solids, J. Appl. Phys. I (1990). edited by Krieger and Malabar, FL.
[37] H. McSkimin, P. Andreacht, Measurement of 3-order moduli of silicon and germmanium, J. Appl. Phys. 35 (1964) 3312–&.
[38] G.J.A.B.B. Karki, J. Crain, Si under compression, J. Phys.: Condens. Matter 9 (1997) 8579.
[39] R.E. Cohen, L. Stixrude, E. Wasserman, Tight-binding computations of elastic anisotropy of Fe, Xe, and Si under compression, Phys. Rev. B 56 (1997) 8575–8589.
[40] B.A. Landolt, Crystal and solid state physics, in: K. Hellwege (Ed.), Landolt-Brnstein New Series, Group X, vol. 11, 1979, p. 116.
[41] C. Guminski, Hg–Re (mercury–rhenium), J. Phase Equilib. 23 (2002) 184–185.
[42] C. Guminski, The C–Hg (carbon–mercury) system, J. Phase Equilib. 14 (1993) 219–220.
[43] A. Dewaele, J. Eggert, P. Loubeyre, R. Le Toullec, Measurement of refractive index and equation of state in dense He, H-2, H_2O, and Ne under high pressure in a diamond anvil cell, Phys. Rev. B 67 (2003).
[44] P.W. Bridgman, The action of mercury on steel at high pressures, Proc. Am. Acad. Arts Sci. 46 (1911) 325–341.
[45] C.R. Tilford, The speed of sound in a mercury ultrasonic interferometer manometer, Metrologia 24 (1987) 121.
[46] L.A. Davies, R.B. Gordon, The speed of sound in a mercury, J. Chem. Phys. 46 (1967) 2650.
[47] J. Daridon, B. Lagourette, J.-P. Grolier, Experimental measurements of the speed of sound in *n*-hexane from 293 to 373 K and up to 150 MPa, Int. J. Thermophys. 19 (1998) 145–160.
[48] S. Lago, G. Albo, A new method to calculate the thermodynamical properties of liquids from accurate speed-of-sound measurements, J. Chem. Thermodynam. 40 (2008) 1558–1564.
[49] M.J. Dávila, J. Martin Trusler, Thermodynamic properties of mixtures of ⟨i⟩ n⟨/i⟩-methyl-2-pyrrolidinone and methanol at temperatures between 298.15 K and 343.15 K and pressures up to 60 MPa, J. Chem. Thermodynam. 41 (2009) 35–45.
[50] N. Fletcher, Adiabatic assumption for wave propagation, Am. J. Phys. 42 (1974) 487.
[51] G. Holman, C. Ten Seldam, A critical evaluation of the thermophysical properties of mercury, J. Phys. Chem. Ref. Data 23 (1994) 807–827.
[52] T. Grindley, J.E. Lind Jr, Pvt properties of water and mercury, J. Chem. Phys. 54 (1971) 3983.
[53] O. Kleppa, Ultrasonic velocities of sound in some metallic liquids. Adiabatic and isothermal compressibilities of liquid metals at their melting points, J. Chem. Phys. 18 (1950) 1331.
[54] J.R. MacDonald, Review of some experimental and analytical equations of state, Rev. Mod. Phys. 41 (1969) 316–349.
[55] P.B. Roy, S.B. Roy, Applicability of isothermal unrealistic two-parameter equations of state for solids, J. Phys.: Condens. Matter 18 (2006) 10481.
[56] F. Birch, The effect of pressure upon the elastic parameters of isotropic solids, according to Murnaghan's theory of finite strain, J. Appl. Phys. 9 (1938).
[57] F. Birch, Finite strain isotherm and velocities for single-crystal and poly-crystalline NaCl at high pressures and 300 K, J. Geophys. Res. 83 (1978) 1257.
[58] J.-X. Sun, Q. Wu, L.-C. Cai, F.-Q. Jing, Equation of state for solids with high accuracy and satisfying the limitation condition at high pressure, Phys. B: Condens. Matter 371 (2006) 257–271.
[59] P. Vinet, J.H. Rose, J. Ferrante, J.R. Smith, Universal features of the equation of state of solids, J. Phys.: Condens. Matter 1 (1989) 1941.
[60] W.B. Holzapfel, Equations of state for ideal and real solids under strong compression, EPL (Europhys. Lett.) 16 (1991) 67.
[61] W. Klement, A. Jayaraman, G.C. Kennedy, Transformations in mercury at high pressures, Phys. Rev. 131 (1963) 1–6.

Please cite this article in press as: F. Decremps et al., Picosecond acoustics method for measuring the thermodynamical properties of solids and liquids at high pressure and high temperature, Ultrasonics (2014), http://dx.doi.org/10.1016/j.ultras.2014.04.011